Hindawi
Shock and Vibration
Volume 2021, Article ID 6674351, 18 pages
https://doi.org/10.1155/2021/6674351

Research Article

Hydraulic Pump Fault Diagnosis Method Based on EWT Decomposition Denoising and Deep Learning on Cloud Platform

Wanlu Jiang,[1,2] Zhenbao Li,[1,2] Sheng Zhang,[1,2] Teng Wang,[1,2] and Shuqing Zhang[3]

[1]*Hebei Provincial Key Laboratory of Heavy Machinery Fluid Power Transmission and Control, Yanshan University, Qinhuangdao, Hebei 066004, China*
[2]*Key Laboratory of Advanced Forging & Stamping Technology and Science, Yanshan University, Ministry of Education of China, Qinhuangdao, Hebei 066004, China*
[3]*School of Electrical Engineering, Yanshan University, Qinhuangdao, Hebei 066004, China*

Correspondence should be addressed to Zhenbao Li; lizhenbao_ysu@163.com

Received 29 October 2020; Revised 17 November 2020; Accepted 23 February 2021; Published 12 March 2021

Academic Editor: Ling Zhou

An axial piston pump fault diagnosis algorithm based on empirical wavelet transform (EWT) and one-dimensional convolutional neural network (1D-CNN) is presented. The fault vibration signals and pressure signals of axial piston pump are taken as the analysis objects. Firstly, the original signals are decomposed by EWT, and each signal component is screened and reconstructed according to the energy characteristics. Then, the time-domain features and the frequency-domain features of the denoised signal are extracted, and features of time domain and frequency domain are fused. Finally, the 1D-CNN model was deployed to the WISE-Platform as a Service (WISE-PaaS) cloud platform to realize the real-time fault diagnosis of axial piston pump based on the cloud platform. Compared with ensemble empirical mode decomposition (EEMD) and complementary ensemble empirical mode decomposition (CEEMD), the results show that the axial piston pump fault diagnosis algorithm based on EWT and 1D-CNN has higher fault identification accuracy.

1. Introduction

With the development of industry modernization and information technology, hydraulic technology is more and more widely used in all walks of life. Because the hydraulic system has the advantages of large output power, high work efficiency, high motion accuracy, and stable work [1], the hydraulic system has been widely used from national defense equipment to civilian equipment. The core executive components of most equipment are driven by hydraulic systems, so the performance of the equipment directly depends on the working conditions of the hydraulic system.

Hydraulic system faults have the characteristics of concealed form, high incidence, high damage, and difficult maintenance. Therefore, obtaining fault knowledge and identifying fault characteristics are the focus and difficulty of hydraulic system fault diagnosis research [2–5]. At present, the fault diagnosis problems of hydraulic systems are mainly concentrated in three aspects: first of all, the original signal of the hydraulic system is mixed with a lot of noise signals; secondly, there is a lack of fault diagnosis models with good generalization ability; thirdly, there is a lack of a unified solution for device management and fault diagnosis based on the cloud platform.

Vibration signal processing has always been the research hotspot of signal processing methods, which is very important for equipment vibration signal detection and fault diagnosis [6–8]. There are two main types of vibration signal processing methods: one is traditional methods such as amplitude domain analysis [9], Fourier transform [10], and other methods; and the other is more modern methods, such as Wigner-Ville distribution [11], spectrum analysis [12], and wavelet analysis [13]. The current vibration signal decomposition methods mainly include wavelet packet decomposition, Ensemble Empirical Mode Decomposition (EEMD), Complementary Ensemble Empirical Mode

Decomposition (CEEMD), and other methods. However, when the signal has noise, the calculation amount of the algorithm is relatively large, and the signal decomposition effect is not ideal, and it cannot overcome the modal aliasing phenomenon in the signal decomposition process [14]. Therefore, French researcher Gilles combined the advantages of adaptive empirical mode decomposition and wavelet analysis theory to propose a method named Empirical Wavelet Transform (EWT) algorithm [15]. Therefore, research scholars at home and abroad have applied the EWT algorithm as a new signal processing and analysis tool to some nonstationary signal research and achieved good results [16, 17]. The EWT method has a good decomposition effect on multimodal and noisy signals and can eliminate the problem of modal aliasing. The modal components extracted by it are AM and FM signals containing a certain frequency band. EWT is more robust than the modes extracted by EEMD and CEEMD. Comparing EWT with EEMD and CEEMD methods, the effectiveness of EWT is verified through simulation and test results.

In recent years, scholars at home and abroad have conducted a lot of research on hydraulic system fault diagnosis technology. Chai et al. [18] proposed a hydraulic system fault diagnosis method combining principal component analysis (PCA) and a kernel extreme learning machine (KELM), which solved the difficult problem of feature extraction and fault diagnosis in the multifault state of the hydraulic system; Tang et al. [19] proposed a method for fault diagnosis of piston pumps based on information fusion, which realized the fault diagnosis by fusing the vibration signals and pressure signal of the axial piston pump into the characteristic layer; Wang and Xiang [20, 21] proposed a convolutional neural network (CNN) method based on minimum entropy deconvolution (MED) and a method using a deep belief network (DBN). By using the deep learning method, the fault diagnosis of the axial piston pump has played a good effect. Liu et al. [22] proposed a fault diagnosis method for piston pumps based on multiple information intensity features; Jiang et al. [23] proposed an axial piston pump fault based on Mel-Frequency Cepstral Coefficient (MFCC) and extreme learning machine (ELM) diagnosis method. Most of the previous fault diagnosis algorithms are based on traditional classification models. However, the complex and changeable working environment of the axial piston pump makes the traditional fault diagnosis algorithms lack adaptability and not able to solve more complicated fault diagnosis problems. With the rapid development of new-generation information technologies such as big data, deep learning, cloud computing, and the Internet of Things, traditional manufacturing is facing the objective needs of digitized, networked, and intelligentized transformation and upgrading. Therefore, the urgent need for informatization in the manufacturing industry and the trend of accelerating the penetration of information technology into the manufacturing field have merged with each other, which has triggered a new round of industrial revolution.

In recent years, deep learning has achieved great success in the fields of natural language processing, computer vision, and image recognition. Deep learning algorithms can learn features adaptively and have powerful feature extraction and characterization capabilities, so they are widely used in the field of fault diagnosis [24]. For example, Chen et al. [25] used deep neural networks to evaluate the deterioration degree of rolling bearings; Lei et al. [26] used deep learning algorithms to achieve health management of multistage gear transmission systems; Sun et al. [27] proposed a fault diagnosis method for induction motors based on sparse autoencoders. The CNN algorithm in deep learning has also been widely used in the fault diagnosis of gearboxes [28] and rolling bearings [29, 30] and has achieved ideal diagnostic results. However, the fault diagnosis method of axial piston pump based on one-dimensional convolutional neural network (1D-CNN) is rarely reported. Therefore, this article applies 1D-CNN to the fault diagnosis of the axial piston pump to improve the accuracy of the axial piston pump fault diagnosis algorithm.

The traditional fault diagnosis method has many disadvantages, such as low efficiency, high hardware cost, and single fault alarm form [31]. At present, remote query of industrial field data is basically impossible. At this stage, the application of equipment remote monitoring and fault diagnosis systems is mainly concentrated in some areas, such as bearing fault diagnosis of wind turbine and fault diagnosis of intelligent vehicle control system. In these areas, remote fault diagnosis systems that use production equipment in the production workshop as the application object are even more rare [32]. However, there are more and more demands for equipment remote monitoring, fault diagnosis, and alarm systems at home and abroad, so the equipment health management system based on cloud platform has become the focus of attention and research in recent years [33].

There are many types of hydraulic system failures, and the causes of failures are more complicated than other common mechanical failures. At present, the maintenance of the hydraulic system still adopts the old strategy of regular inspection and overhaul by maintenance personnel. This maintenance system has high operating costs and cannot cope with potential equipment failures. However, the hydraulic equipment health status cloud management system, through continuous monitoring and analysis of equipment operating data, can evaluate the health status of the equipment in real time, provide early warning of upcoming failures, and even further forcibly stop its operation to reduce property loss. In addition, through the industrial cloud platform, the type of failure can be identified in a short time, and then maintenance or repair programs can be provided to users to reduce equipment downtime.

With the wide application of hydraulic systems, higher requirements are put forward for the operation stability and timely troubleshooting of hydraulic pumps. In order to reduce the maintenance cost of hydraulic equipment and realize the real-time monitoring and fault diagnosis of the working status of the axial piston pump, this paper proposes a hydraulic pump fault diagnosis method based on deep learning and cloud platform. This method samplings the vibration signals and pressure signal of the axial piston pump in real time. Apply EWT-based methods to

decompose and denoise vibration signals and pressure signals. After denoising, extract the time-domain features of the vibration signals and pressure signal and extract the frequency-domain features of the energy of each subband according to the wavelet packet decomposition theory. Time-domain and frequency-domain features are fused and transmitted to the cloud platform in real time. Apply 1D-CNN on the cloud platform to realize the condition monitoring and fault diagnosis of the axial piston pump. At the same time, the fault diagnosis results will be displayed on the WISE-PaaS cloud platform in real time.

In order to realize the fault diagnosis of axial piston pump accurately, the fault diagnosis algorithm is deployed to the cloud platform to realize the visual display of fault diagnosis results on the cloud. The main contents and structure of this paper are as follows: Section 1 introduces the background of the subject and the purpose and significance of the research. In Section 2, a signal denoising algorithm based on EWT and energy characteristics is proposed. The simulation signal is used for testing. The algorithm has a good denoising effect. Section 3 discusses extraction and fusion of time-domain and frequency-domain characteristics of axial piston pump vibration signals and pressure signal. In Section 4, a fault diagnosis algorithm of axial piston pump based on 1D-CNN is proposed. Section 5 studies the axial piston pump fault diagnosis algorithm based on EWT and CNN and applies it to axial piston pump fault diagnosis, verifies the effectiveness of the method proposed in this paper, and realizes the cloud platform deployment of fault diagnosis algorithm and cloud platform visual release of diagnosis results.

2. Signal Denoising Algorithm Based on Empirical Wavelet Transform

The core of EWT is adaptive segmentation of the Fourier spectrum of the original signal. A suitable orthogonal wavelet filter bank is constructed. Then the AM-FM component with the tightly supported Fourier spectrum is extracted. In order to solve the problem that hydraulic pump vibration signal is easy to be interfered by noise, a combined noise reduction method based on EWT and energy index is proposed. Firstly, EWT method is applied to decompose the original vibration signal. Then, according to the energy index, the decomposed Intrinsic Mode Function (IMF) is screened and reconstructed, so as to achieve the original signal denoising.

2.1. Empirical Wavelet Transform. EWT divides the signal on the Fourier spectrum and then establishes a filter for filtering. In the frequency domain, suppose that the angular frequency of the signal is $\omega(\omega \in [0, \pi])$, and decompose $[0, \pi]$ into N intervals of different bandwidths. This interval is called Λ_n, and each segment is expressed as

$$\Lambda_n = [\omega_{n-1}, \omega_n], n = 1, 2, \ldots, N, \tag{1}$$

$$U_{n=1}^{N} \Lambda_n = [0, \pi], \tag{2}$$

with each ω_n as the center; a transition section is defined, and the width of the transition section is $T_n = 2\tau_n$, as shown in Figure 1.

After confirming interval Λ_n, the band-pass filter on each Λ_n is an empirical wavelet. According to the definition method of wavelet theory, all empirical wavelet is constructed. The definitions of empirical wavelet scaling function $\widehat{\varphi}_n(\omega)$ and wavelet function $\widehat{\psi}_n(\omega)$ in the frequency domain can be expressed as

$$\widehat{\varphi}_n(\omega) = \begin{cases} 1; \text{if } |\omega| \le (1-\gamma)\omega_n, \\ \cos\left[\frac{\pi}{2}\beta\left(\frac{1}{2\gamma\omega_n}\left(|\omega| - (1-\gamma)\omega_n\right)\right)\right]; \text{if } (1-\gamma)\omega_n \le |\omega| \le (1+\gamma)\omega_n, \\ 0; \text{ otherwise}, \end{cases} \tag{3}$$

$$\widehat{\psi}_n(\omega) = \begin{cases} 1; \text{if } (1+\gamma)\omega_n \le |\omega| \le (1-\gamma)\omega_{n+1} \\ \cos\left[\frac{\pi}{2}\beta\left(\frac{1}{2\gamma\omega_{n+1}}\left(|\omega| - (1-\gamma)\omega_{n+1}\right)\right)\right]; \text{if } (1-\gamma)\omega_{n+1} \le |\omega| \le (1+\gamma)\omega_{n+1}, \\ \sin\left[\frac{\pi}{2}\beta\left(\frac{1}{2\gamma\omega_n}\left(|\omega| - (1-\gamma)\omega_n\right)\right)\right]; \text{if } (1-\gamma)\omega_n \le |\omega| \le (1+\gamma)\omega_n, \\ 0; \text{ otherwise}, \end{cases} \tag{4}$$

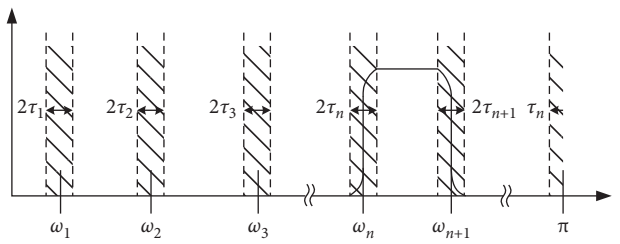

Figure 1: Frequency band distribution.

where $0 < \gamma < 1$, $\tau_n = \gamma\omega_n$, and $(\gamma < \min_n(\omega_{n+1} - \omega_n/\omega_{n+1} + \omega_n))$; according to the literature [34], $\beta(x) = x^4(35 - 84x + 70x^2 - 20x^3)$.

The key in EWT algorithm process is to divide the Fourier spectrum. There are N consecutive bandwidths in the range of 0 to π, where $\omega_0 = 0$ and $\omega_N = \pi$. The remaining $(N-1)$ boundaries are determined by searching the local maximum values of the spectrum [15]. Mark M as the number of maxima; when $M \geq N$, the first $N-1$ maxima are retained, and when $M < N$, all maxima are retained and N is modified. Finally, the intermediate frequency between two local maxima is taken as $\omega_n (n = 1, 2, \ldots, N-1)$.

In this regard, mark the original signal as $f(t)$, whose spectrum is $\widehat{f}(\omega)$. According to the traditional wavelet transform method, the empirical wavelet transform $W_f^e(n,t)$ is defined, and the Fourier transform and the inverse transform are denoted as $F[\cdot]$ and $F^{-1}[\cdot]$, respectively. Then the detailed coefficient and approximate coefficient are, respectively,

$$W_f^e(n,t) = \langle f(t), \psi_n(t)\rangle = \int f(\tau)\overline{\psi_n(\tau - t)}\mathrm{d}\tau = F^{-1}\left[\hat{f}(\omega)\overline{\overset{\wedge}{\psi}_n(\omega)}\right], \tag{5}$$

$$W_f^e(0,t) = \langle f(t), \varphi_1(t)\rangle = \int f(\tau)\overline{\varphi_1(\tau - t)}\mathrm{d}\tau = F^{-1}\left[\hat{f}(\omega)\overline{\overset{\wedge}{\varphi}_1(\omega)}\right]. \tag{6}$$

In the above equations, $\psi_n(t)$ is the empirical wavelet function; $\varphi_1(t)$ is the scale function; $\widehat{\psi}_n(\omega)$ and $\widehat{\varphi}_1(\omega)$ are the Fourier transforms of $\psi_n(t)$ and $\varphi_1(t)$, respectively; $\overline{\psi_n(t)}$ and $\overline{\varphi_1(t)}$ are the complex conjugates of $\psi_n(t)$ and $\varphi_1(t)$, respectively. The reconstruction of the original signal is

$$\begin{aligned} f(t) &= W_f^e(0,t) * \varphi_1(t) + \sum_{n=1}^{N} W_f^e(n,t) * \psi_n(t) \\ &= F^{-1}\left[\widehat{W}_f^e(0,\omega)\widehat{\varphi}_1(\omega) + \sum_{n=1}^{N}\widehat{W}_f^e(n,\omega)\widehat{\psi}_n(\omega)\right]. \end{aligned} \tag{7}$$

In the above equation, the symbol $*$ represents convolution. $\widehat{W}_f^e(0,\omega)$ and $\widehat{W}_f^e(n,\omega)$ are the Fourier transforms of $W_f^e(0,t)$ and $W_f^e(n,t)$, respectively. The mode components of the empirical wavelet transform are defined as follows:

$$f_0(t) = W_f^e(0,t) * \varphi_1(t), \tag{8}$$

$$f_n(t) = W_f^e(n,t) * \psi_n(t), \quad n = 1, 2, \ldots, N. \tag{9}$$

The mode components obtained by the empirical wavelet transform are subjected to Hilbert transform to obtain the relevant instantaneous frequency and instantaneous amplitude. Finally, the time-frequency distribution of the signal can be obtained.

2.2. Using Energy Value as an Evaluation Index of Vibration Signal Denoising. In the early stage of failure of the hydraulic pump, due to the high-speed rotation of the machine, periodic vibration and shock will occur. Therefore, the signal energy value can be used to characterize the proportion of information carried by each IMF component after signal decomposition. After calculating the energy proportion of each IMF component, the IMF components are rearranged in descending order according to the energy proportion. The IMF components with accumulated energy ≥80% are reconstructed to obtain denoised vibration signals and pressure signals. The energy calculation formula of n-th IMF component is as follows:

$$E_n = \sum_{i=1}^{K} f_n(i)^2, \tag{10}$$

where $f_n(t)$ represents the n-th IMF component after decomposition of the original signal. K is the number of sample points of the original signal.

2.3. Simulation Signal Analysis. In order to verify the effectiveness of the denoising algorithm, signals $f_{\mathrm{sig}}(t)$ with different frequencies and different amplitudes were artificially simulated. Add 15 dB Gaussian white noise to the signal $f_{\mathrm{sig}}(t)$ to obtain the signal $f_o(t)$ to be denoised.

$$f_{\mathrm{sig}}(t) = \cos(6\pi t) + 2\cos(40\pi t) + 0.5\cos\left(20\pi t + 10\pi t^2\right), \tag{11}$$

$$f_o(t) = f_{\mathrm{sig}}(t) + noise \tag{12}$$

Among them, *noise* represents the added noise and the signal-to-noise ratio (SNR) = 15 dB. The original signal and the signal after adding noise are shown in Figure 2.

Use EWT to decompose the noisy signal $f_o(t)$. After decomposition, the IMF components with cumulative

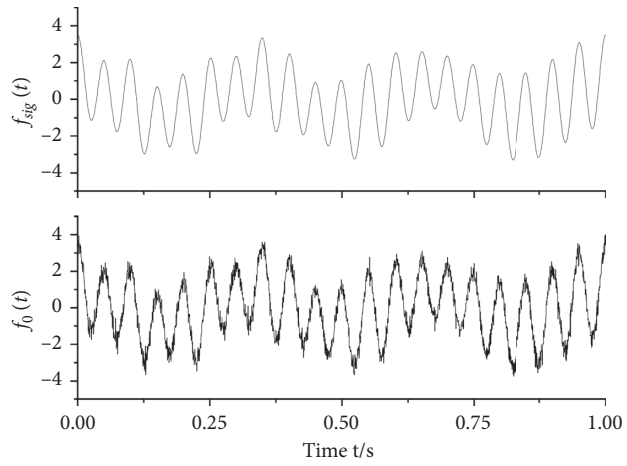

Figure 2: Time-domain diagram of $f_{sig}(t)$ signal and $f_o(t)$ signal.

energy ≥80% are extracted and reconstructed to obtain the simulated signal after noise reduction. In order to verify the effectiveness of the denoising method proposed in this paper, the EEMD and CEEMD methods are used to decompose and denoise the original noise signal $f_o(t)$ [1]. The comparison of denoising effects is shown in Figure 3.

In Figure 3, the methods based on EEMD and CEEMD have poor reconstruction effects on the original signal after decomposition and denoising. The energy criterion adopted in this paper as the selection criterion of IMF components led CEEMD denoising method eliminates part of the original signal, so its SNR is lower than 15 dB. Meanwhile, the signal denoising method based on EWT can effectively denoise the original signal. In order to be able to quantitatively analyze the effects of the three signal denoising methods, this paper compares the SNR of the three denoising signals, as shown in Table 1. The SNR of the signal denoising method based on EWT is obviously higher than the other two methods; it proves the effectiveness of the EWT-based signal denoising method proposed in this paper.

3. Feature Extraction and Feature Fusion

3.1. Time-Domain Feature Extraction. Time-domain analysis methods include amplitude-domain analysis and correlation analysis. When a hydraulic pump fails, the statistical characteristic parameters of the amplitude of its vibration signal and pressure signal will also change with the type of its failure. Therefore, the amplitude-domain statistical analysis can be used for the fault diagnosis of the axial piston pump [35]. Table 2 shows common statistics used to describe signal characteristics in the time domain. Suppose that the original signal $f(i)$ is denoised and the denoised signal $x(i)$ is obtained, where $i = 1, 2, 3, \ldots, K$, and K is the number of sample points of the original signal.

3.2. Frequency-Domain Feature Extraction. Compared with the wavelet transform, the wavelet packet transform has improved the ability of the frequency-domain localization of the signal. The application of the wavelet packet decomposition can realize a more comprehensive frequency-domain analysis of the signal. The wavelet packet

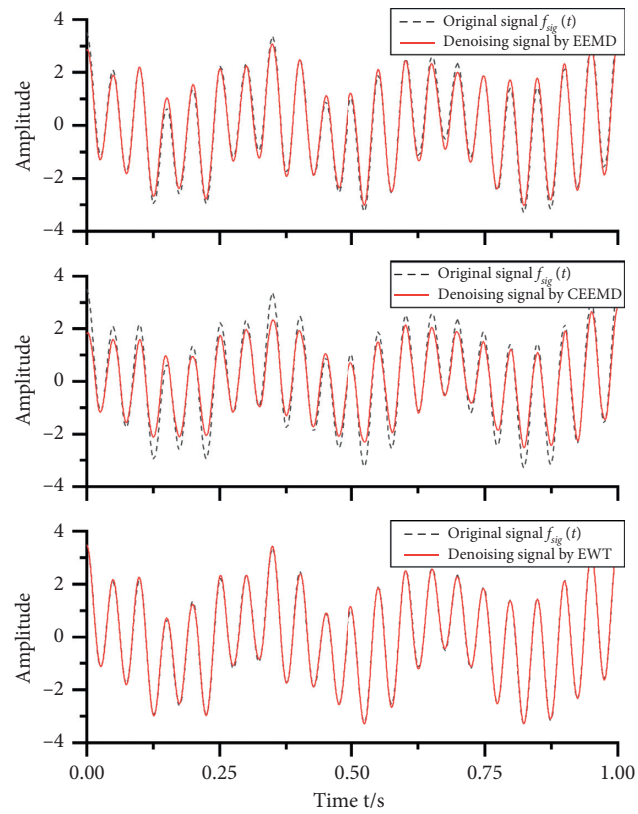

Figure 3: Comparison of denoising effects of simulated signals.

Table 1: SNR comparison analysis.

Denoising method	EEMD	CEEMD	EWT
Signal-to-noise ratio (SNR)/dB	18.07	12.22	28.38

decomposition of the vibration and pressure denoised signal can extract the energy characteristics of each frequency band as the frequency-domain characteristics of the signal.

The signals were decomposed by three-layer wavelet packet, and the decomposition tree structure is shown in Figure 4. Three-layer wavelet packet decomposition was performed on the denoised signal $x(i)$. The formula for calculating the signal energy at n-th node of the wavelet packet is

$$E_n = \sum_{i=1}^{K} x_n(i)^2. \tag{13}$$

In the above equation, $x_n(i)$ is the reconstructed signal at the n-th node of the wavelet packet, $n = 1, 2, \ldots, 8$, and K is the number of sample points of the original signal.

After the wavelet packet decomposition, the subbands are rearranged, and the corresponding relationship between the wavelet packet nodes and energy features is shown in Table 3.

4. Fault Recognition Method Based on Convolutional Neural Network

The neural network approximates a large number of neurons to fit nonlinear relationships by organization and update.

Table 2: Time-domain feature extraction method.

Time-domain statistical characteristics	Time-domain statistical feature calculation formula
Mean	$P_1 = \sum_{i=1}^{K} x(i)/K$
Absolute mean	$P_2 = \sum_{i=1}^{K} \lvert x(i)\rvert/K$
Effective value	$P_3 = \sqrt{\sum_{i=1}^{K} [x(i)]^2/K}$
Average power	$P_4 = \sum_{i=1}^{K} [x(i)]^2/K$
RMS	$P_5 = (\sum_{i=1}^{K} \sqrt{\lvert x(i)\rvert}/K)^2$
Peak	$P_6 = \max(\lvert x(i)\rvert)$
Peak-to-peak	$P_7 = \max[x(i)] - \min[x(i)]$
Variance	$P_8 = \sum_{i=1}^{K} [x(i) - P_1]^2/(K-1)$
Standard deviation	$P_9 = \sqrt{\sum_{i=1}^{K} [x(i) - P_1]^2/(K-1)}$
Skewness	$P_{10} = \sum_{i=1}^{K} [x(i) - P_1]^3/K$
Kurtosis	$P_{11} = \sum_{i=1}^{K} [x(i) - P_1]^4/K$
Shape factor	$P_{12} = P_3/P_2$
Crest factor	$P_{13} = P_6/P_3$
Impulse factor	$P_{14} = P_6/P_2$
Clearance factor	$P_{15} = P_6/P_5$
Skewness factor	$P_{16} = P_{10}/P_9^3$
Kurtosis factor	$P_{17} = P_{11}/P_9^4$

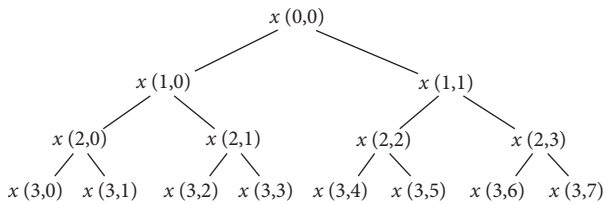

Figure 4: Three-layer decomposition tree structure of wavelet packet.

Table 3: Correspondence between wavelet packet nodes and energy features.

Node	Energy characteristics
$x(3,0)$	E_1
$x(3,1)$	E_2
$x(3,2)$	E_4
$x(3,3)$	E_3
$x(3,4)$	E_7
$x(3,5)$	E_8
$x(3,6)$	E_6
$x(3,7)$	E_5

With this advantage, it is applied to various fields and has achieved great success [36]. CNN conducts data training through the convolution layer and pooling layer. When using it for training, it is not necessary to perform explicit feature extraction but to complete learning through training data in an implicit manner. The convolutional neural network is inspired by biology, and its layout structure is more like a real biological neural network. Its weight sharing makes the network simpler, especially with the feature that the image of multidimensional input vector can be directly input into the network, which avoids the complexity of data reconstruction in the process of feature extraction and classification [37]. CNN has unique advantages in speech, image, and signal processing because of its network structure with local weight sharing. CNN has functions such as local perception and pooling, which are highly invariant to deformations such as translation, tilt, and zoom [38]. Therefore, it is widely used in image, video, and signal processing and other related recognition fields.

4.1. One-Dimensional Convolutional Neural Network Structure. A typical convolutional neural network is initially composed by convolutional layer and pooling layer alternately, and finally fully connected layer is connected before the output layer, as shown in Figure 5. By processing the convolutional layer and the pooling layer, the pixels of the obtained two-dimensional feature map are sequentially spliced and input into the fully connected layer, and finally the classification output is realized in the output layer.

The convolutional neural networks are widely used in the field of image recognition and have unique advantages in signal processing, such as speech signals and time series. The analyzed vibration signal is also a one-dimensional time series, and the input layer, convolution kernel, and learned features are all one-dimensional [39]. The specific structure of 1D-CNN is shown in Figure 6.

The principle of 1D-CNN is to use the convolution kernel to move along the input sample to obtain the characteristics of the input sample and form a feature vector. In this way, because the weights of the convolution kernel are different, the feature vectors obtained are not the same. In the convolutional layer, the convolution kernel extracts the same feature on each sequence segment of the input sample. Then it performs local connection and weight sharing, so that there is no need to consider the particularity of the local location, which greatly

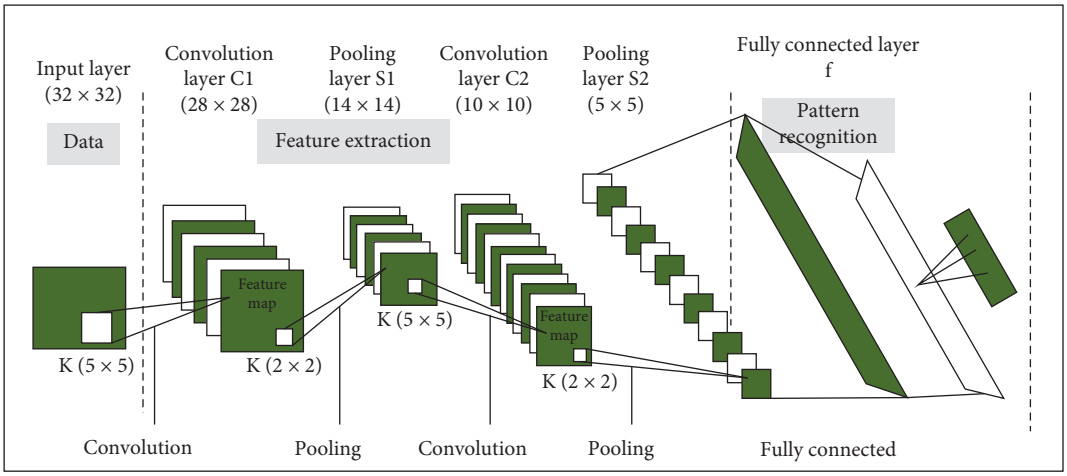

Figure 5: Typical convolutional neural network structure diagram.

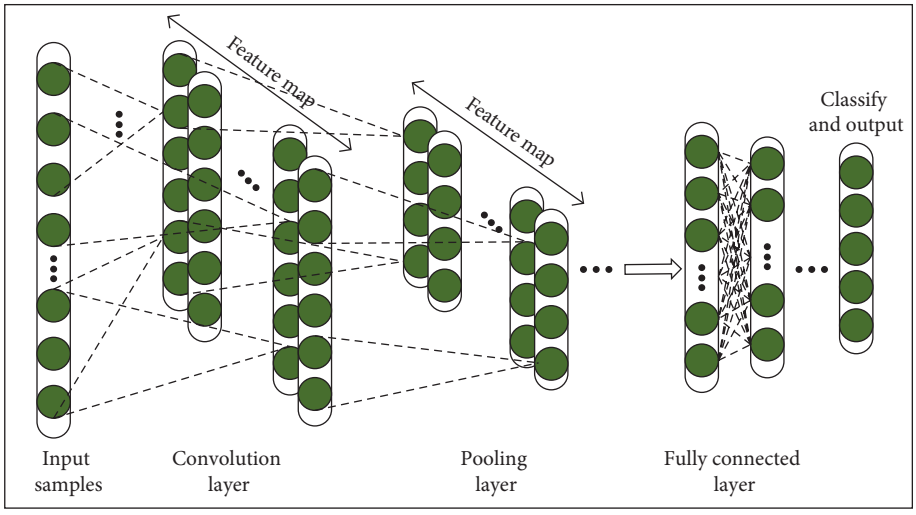

Figure 6: One-dimensional convolutional neural network structure diagram.

reduces the network parameters. Because the weight of the convolution kernel is different, the network can get different information at the same position of the sample. In CNN, the convolutional layer and the pooling layer are closely connected. The pooling layer can reduce the sensitivity of the network output to translation and zooming, making the classification task easier.

4.2. Convolutional Layer. The convolutional layer of neural network has more than one convolution kernel as the local receptive field for learning data feature. Each convolution kernel will act on the entire receptive field multiple times and weight sharing can also be used to reduce the amount of network parameters.

In the convolutional layer, the convolution kernel performs a convolution operation on the feature vector output by the previous layer and uses a nonlinear activation function to construct the output feature vector. The output of each layer is the convolution result of multiple input features, and the calculation process is [40]

$$\mathbf{X}_{\mathrm{cm}}^{l} = f_1\left(\sum_{\mathbf{X}_n^{l-1}\in M_m} \mathbf{X}_n^{l-1} * \mathbf{K}_{\mathrm{nm}}^{l} + b_{\mathrm{cm}}^{l}\right). \tag{14}$$

In the above equation, $\mathbf{X}_{\mathrm{cm}}^{l}$ represents the m-th feature map obtained after activation of the l-th convolutional layer; $f_1(\cdot)$ is the activation function of convolutional layer; $\mathbf{K}_{\mathrm{nm}}^{l}$ is the convolution kernel connecting the n-th feature map in layer l-1 and the m-th feature map in layer l; b_{cm}^{l} is the bias of the m-th feature map of the l-th convolutional layer; M_m is the set of selected input feature maps. In this paper, the Rectified Linear Unit (ReLU) was selected as the activation function $f_1(\cdot)$. The advantage of ReLU is to make the output of some neurons be 0, which improves the sparsity of the network and reduces the interdependence of parameters, which relieves occurrence of overfitting problem.

4.3. Pooling Layer. Generally, the feature map obtained after processing by the convolutional network has a large dimension, which makes subsequent classification difficult to

perform. Therefore, a downsampling layer is usually followed after the convolutional layer, which is also called a pooling layer. The operation of the pooling layer can not only reduce the dimension of features but also ensure the invariance of feature positions [39]. The representation is

$$\mathbf{X}_{\mathrm{pm}}^{l} = f_2\left[w_m^l \mathrm{down}\left(\mathbf{X}_{\mathrm{cm}}^{l}\right) + b_{\mathrm{pm}}^{l}\right], \tag{15}$$

where $\mathbf{X}_{\mathrm{pm}}^{l}$ is the feature map obtained from the m-th pooling of pooling layer l; $f_2(\cdot)$ is the activation function of pooling layer. In this paper, ReLU was selected as the activation function $f_2(\cdot)$; down (.) is the pooling function; w_m^l is the weight of the m-th output feature map in layer l; b_{pm}^{l} is the bias of the feature map obtained from the m-th pooling of pooling layer l.

After the feature map is obtained through the convolutional layer, each feature map is generally pooled. There are two commonly used pooling methods: one is the maximum pooling method, and the other is the average pooling method. They are expressed as follows.

4.3.1. Average Pooling. Take the average value of feature points in the pooling domain, set the matrix of downsampling pooling domain as $t \times t$, and the calculation process is

$$s = \mathrm{down}\left(\mathbf{Out}_{t\times t}\right) = \frac{1}{t \times t}\left(\sum_{i=1}^{t}\sum_{j=1}^{t} \mathrm{out}_{ij}\right), \tag{16}$$

where $\mathbf{Out}_{t\times t}$ is the pooling domain; out_{ij} is the element of i-th row and j-th column of $\mathbf{Out}_{t\times t}$; s is the output value of the characteristic points in the pooled domain obtained after the pooling function.

4.3.2. Maximum Pooling.

$$s = \mathrm{down}\left(\mathbf{Out}_{t\times t}\right) = \max_{i,j\in[1,t]}\left(\mathrm{out}_{ij}\right), \tag{17}$$

where $\max_{i,j\in[1,t]}(\mathrm{out}_{ij})$ is the largest element from the pooled domain.

The maximum pooling sampling method can retain the texture features of the signal in the largest range, while the average pooling sampling method can retain the overall characteristics of the data. Refer to models such as NIN and GoogLeNet, which use maximum pooling in the early stage and average pooling in the later stage. Therefore, this article also uses the method of maximum pooling and then average pooling to build a 1D-CNN model.

4.4. Fully Connected Layer. The output part of CNN includes full connection end to end of the output of the last pooling layer. Finally, the Softmax classifier is used to solve the multiclassification problem. The output of the fully connected layer is

$$\mathbf{x}^{l} = f_3\left(\mathbf{W}^{l}\mathbf{x}^{l-1} + \mathbf{b}^{l}\right). \tag{18}$$

In the above equation, $\mathbf{x}^{l-1}$ is the input vector of fully connected neural network; $\mathbf{x}^{l}$ is the output vector of fully connected neural network; $\mathbf{W}^{l}$ is the weight matrix of layer l; $\mathbf{b}^{l}$ is the bias vector of layer l. $f_3(\cdot)$ is the activation function of fully connected layer. In this paper, ReLU was selected as the activation function $f_3(\cdot)$.

4.5. Dropout Layer. In order to prevent the network from overfitting, the dropout layer is introduced in this article. The dropout layer will randomly deactivate some nodes of the neural network, so that the neural network will not make a neuron's weight too large during the training process. Because the input features of this node may be eliminated, the neural network will not overly rely on any single input feature. In the process of training the neural network containing the dropout layer, the essence is to train multiple subneural networks. Finally, in the process of testing, in order to improve the robustness of the fault diagnosis model, the subneural networks are combined, similar to a voting mechanism for fault diagnosis.

5. Hydraulic Pump Fault Diagnosis System Based on Industrial IoT Cloud Platform

5.1. Axial Piston Pump Failure Simulation Test Bench. The schematic diagram of the fault simulation test bench used in this article is shown in Figure 7. The vane pump supplies oil to the axial piston pump. The axial piston pump provides pressure oil for the system. The test bench can simulate typical faults such as single shoe loosening failure, single shoe slipping failure, single shoe wear failure, swash plate wear failure, and center spring failure to meet the test verification requirements.

During the test, the solenoid valve 16 is energized, and the pilot-operated overflow valve 19 is adjusted to set the system pressure to 15 MPa. The models and performance parameters of the motors, axial piston pumps, sensors, and data acquisition cards selected for this test bench are shown in Table 4.

The hydraulic pump installation arrangement of the test bench adopts the top-mounted type (horizontal type). This arrangement is not only conducive to pump disassembly and fault injection but also conducive to the installation of sensors. The sensor layout is shown in Figure 8.

Throughout the experiment process, the vibration signal and pressure signal of the pump under six different conditions were acquisited, which were the normal working state, single slipper loosing fault, single slipper off fault, single slipper wear fault, swash plate wear fault, and center spring fault. Some pictures of the fault elements are shown in Figure 9.

This experiment uses WebAccess/MCM to compile the data acquisition program and chooses the PCI-1747 data acquisition card produced by Advantech, with the highest sampling frequency of 250 kS/s. During the sampling process, set the sampling frequency to 20 kHz and the sampling time to 1 s. The front panel of the acquisition program is shown in Figure 10.

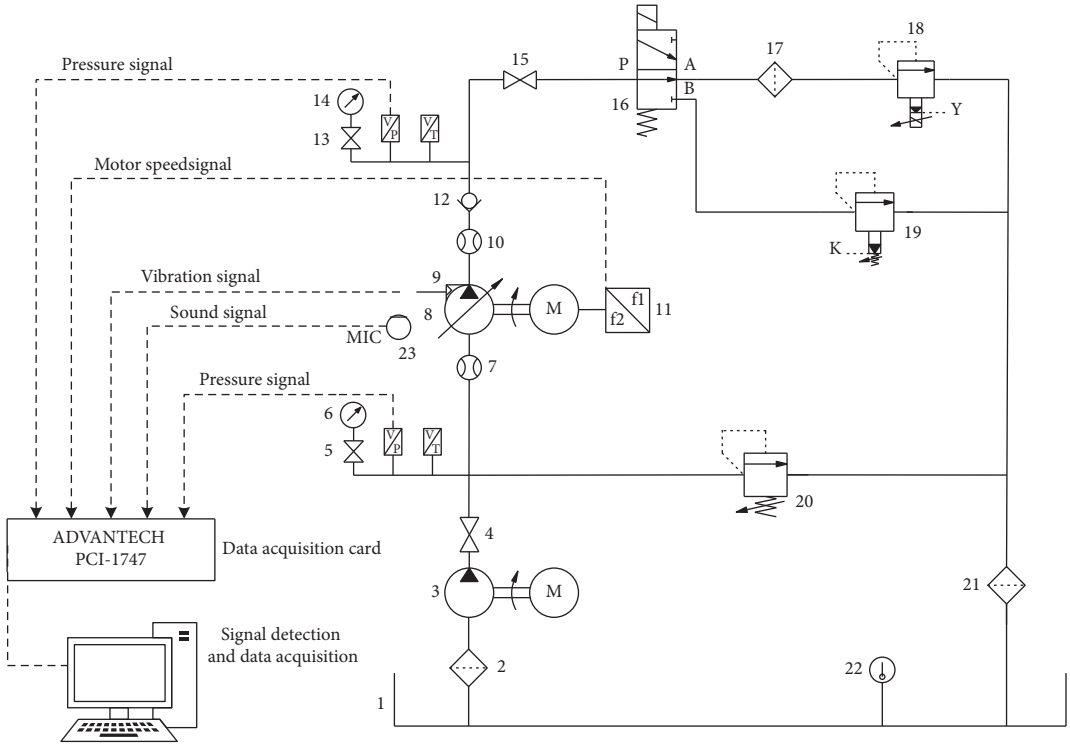

Figure 7: Hydraulic system diagram of hydraulic pump failure simulation test bench. 1, oil tank; 2, 21, and 17, filter; 3, vane pump; 4 and 15, stop valve; 5 and 13, pressure gauge switch; 6 and 14, pressure; 7 and 10, flow meter; 8, axial piston; 9, vibration sensor; 11, frequency converter; 12, check valve; 16, two-position three-way solenoid valve; 18, pilot-operated proportional overflow valve; 19, pilot-operated overflow value; 20, overflow value; 22, temperature meter; 23, impulse sound level meter.

Table 4: Types and performance parameters of test components.

Num.	Component name	Component model	Component performance parameters
1	Motor	Y132M-4	Rated speed: 1480 rpm
2	Axial piston pump	MCY14-1B	Theoretical displacement: 10 ml/r, rated pressure: 31.5 MPa, 7 pistons
3	Data acquisition card	PCI-1747	Maximum sampling rate: 250kS/s
4	Vibration sensor	YD72D	Frequency range: 0.3 Hz–18 kHz
5	Pressure sensor	SYB-351	Measuring range: 0–25 MPa

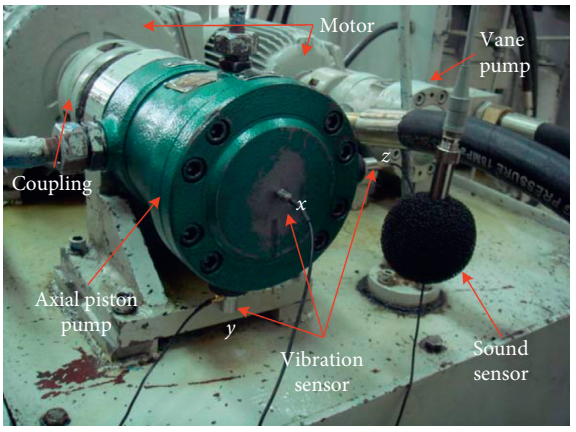

Figure 8: Hydraulic pump failure simulation test bench.

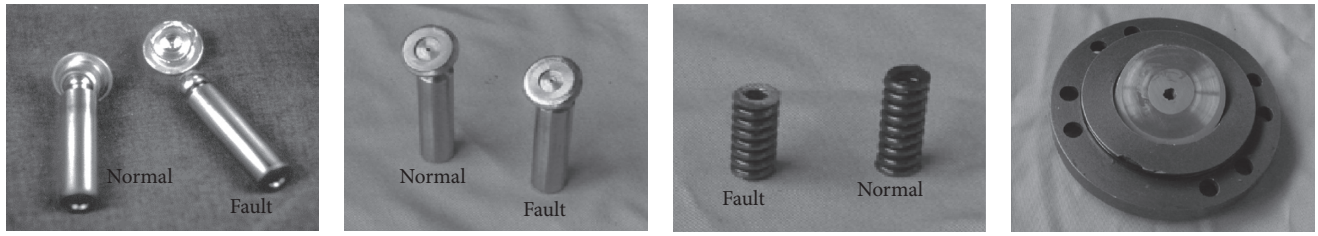

(a) (b) (c) (d)

Figure 9: Some pictures of the fault elements. (a) Single slipper off fault. (b) Single slipper wear fault. (c) Center spring fault. (d) Swash plate wear fault.

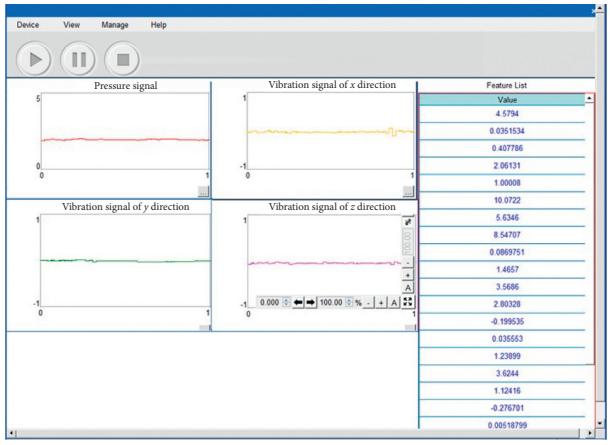

Figure 10: Data acquisition system based on WebAccess/MCM.

5.2. Signal Denoising of EWT Based on IMF Energy Contribution Rate. Intercept part of the pump outlet pressure signal and vibration signals of the single slipper off fault for analysis. Use EWT to decompose and denoise the original signal. The comparison between original signals and denoised signals is shown in Figure 11.

Define the outlet pressure signal of the axial piston pump as p, the axial vibration signal of the axial piston pump as x, the vertical vibration signal as y, and the horizontal vibration signal as z. The layout of the vibration sensor is shown in Figure 12.

In order to study the denoising effect of the three denoising methods against the vibration signal, the x-direction vibration signal under the condition of the swash plate wear fault is analyzed and the denoising results of the three denoising methods are compared, as shown in Figure 13. There are still a large number of redundant noise signals in the signal after EEMD denoising. Although, from the point of view of signal-to-noise ratio, CEEMD algorithm has better denoising effect, its loss to the original signal is relatively large. EWT-based signal denoising methods are better than EEMD and CEEMD methods.

5.3. Feature Extraction and Feature Fusion. The original data used in this paper are all one-dimensional time series signals. Since the prerequisite for implementing the deep learning fault diagnosis algorithm is to have a large number of training samples, this paper adopts the method of overlapping training samples to expand the training data. The segmentation diagram is shown in Figure 14. In this article, the length of each sample is 800 points, and the length of the overlapping part is 600 points.

The test samples are selected from the pressure signal and vibration signals in three directions of the axial piston pump in the normal working state and the five fault states. The specific test sample information is shown in Table 5.

Each sample of the axial piston pump under different working conditions extracts the time-domain characteristic parameters $P_1 - P_{17}$ and frequency-domain characteristic parameters $E_1 - E_8$ of its pressure signal and the three-way vibration signals. Therefore, 25 characteristic parameters can be extracted from each signal. The characteristic parameters of the four signals in each working state of the axial piston pump are connected end to end for feature fusion to form the characteristic vector in the working state.

5.4. Fault Diagnosis Algorithm Based on CNN. The one-dimensional convolutional neural network model used in this article is shown in Figure 15: (1) The input data is the feature vector containing the characteristic parameters of the axial piston pump outlet pressure signal and the vibration signals in the x-, y-, and z-directions, with a dimension of 100. (2) In convolutional layer 1 and convolutional layer 2, respectively, 100 filters with a convolution kernel size of 4 are defined. (3) The maximum pooling layer selects a pooling size of 2. (4) In convolutional layer 3 and convolutional layer 4, respectively, 160 filters with a convolution kernel size of 4 are defined. (5) The average pooling layer chooses a pooling size of 3. (6) The dropout method layer will randomly assign zero weights to neurons in the network, and this article chooses a dropout ratio of 0.5.

The ratio of the training set to the test set is selected as 3 : 2 and the number of iterations is 60. The recognition accuracy rate curves of the training set and the test set are shown in Figure 16. At the same time, the loss function curves of the training set and the test set are shown in Figure 17. Compare the EWT-CNN fault diagnosis algorithm proposed in this paper with the fault diagnosis algorithms based on EEMD-CNN and CEEMD-CNN. The recognition accuracy rates of different fault diagnosis algorithms are shown in Table 6. The EWT-CNN fault

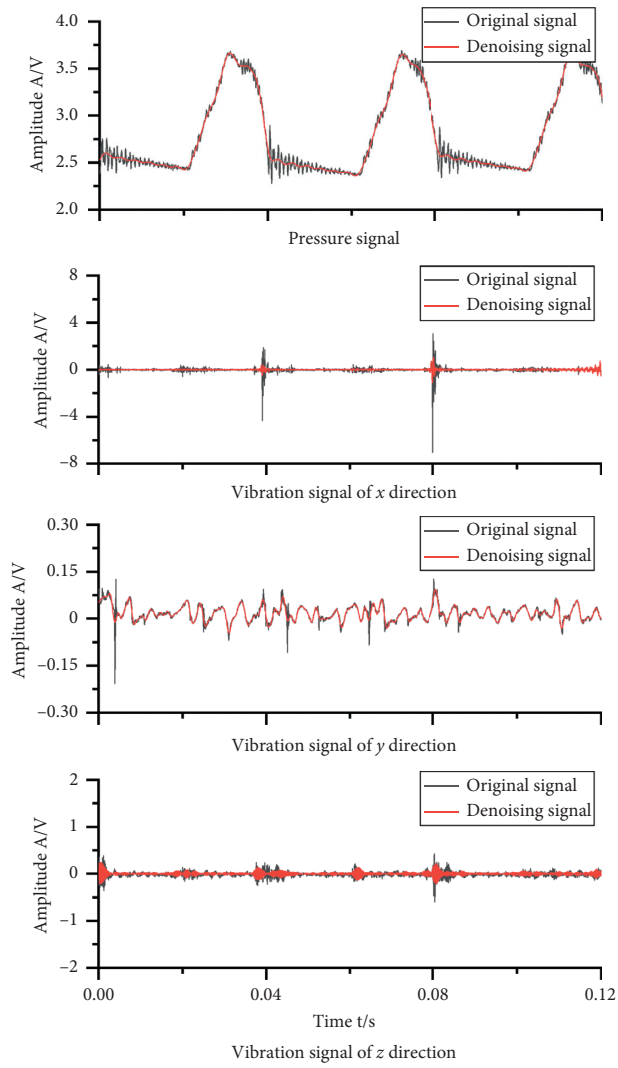

Figure 11: Original signal denoising based on EWT.

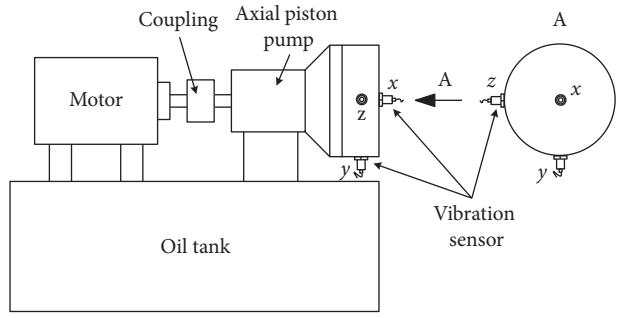

Figure 12: Vibration sensor layout.

diagnosis algorithm proposed in this paper has a significantly higher recognition accuracy than the other two algorithms, and the recognition accuracy rate reaches 99.51%.

In order to verify the axial plunger pump multipath signal characteristic parameters' influence on model identification accuracy rate, the axial piston pump fault diagnosis is carried out only by using the characteristic parameters of the one signal in the pump outlet pressure signal p, x-direction of the vibration signal, y-direction of the vibration signal, and z-direction of the vibration signal. Comparison results are as shown in Figure 18. Comparative analysis shows that the characteristic parameter with the highest accuracy of model recognition is the pump outlet pressure signal p, followed by the x-direction vibration signal. Therefore, axial piston pump outlet pressure signals p and x vibration signals contain more axial piston pump fault information.

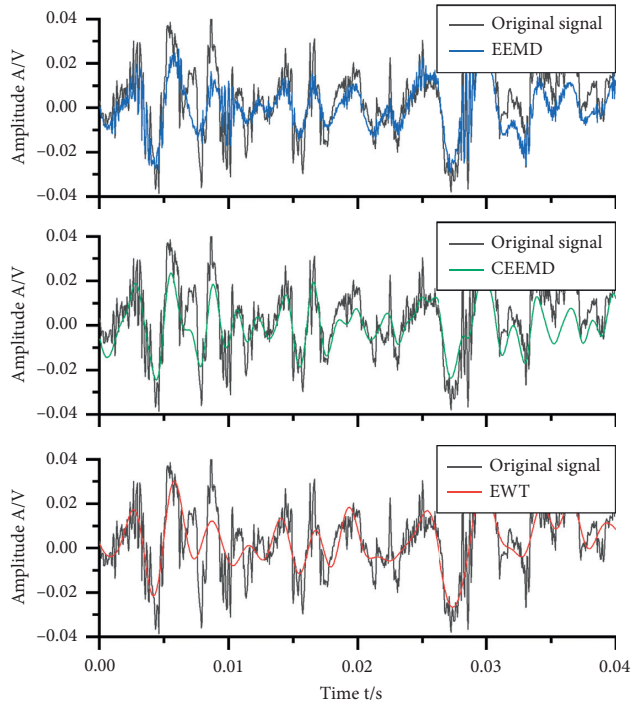

Figure 13: Comparison of denoising effects of three different denoising methods.

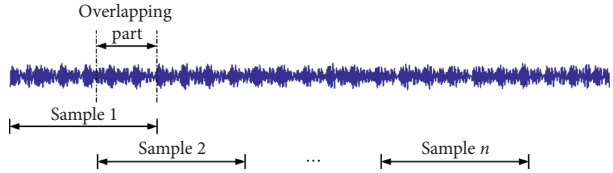

Figure 14: Schematic diagram of sample segmentation.

Table 5: Number of samples and sample labeling method.

Working status	Data length	Feature vector	Sample size	Category mark
Normal working state	800	25 × 4	90	1
Single slipper loosing fault	800	25 × 4	90	2
Single slipper off fault	800	25 × 4	90	3
Single slipper wear fault	800	25 × 4	90	4
Swash plate wear fault	800	25 × 4	90	5
Center spring fault	800	25 × 4	90	6

5.5. t-SNE Visual Analysis. The t-distributed random neighbor embedding (t-SNE) algorithm is currently the best data dimensionality reduction and visualization method. For computers, there is no problem in processing high-dimensional data, but humans can only perceive three dimensions. In order to make the internal processing results of the convolutional neural network be more visualized, it is necessary to visualize high-dimensional data. Therefore, this paper uses the t-SNE algorithm to reduce the dimensionality of the output results of some layers of 1D-CNN into two dimensions for visual display.

Analyze and visualize the features learned from the input layer, convolution layer 2, convolution layer 4, and output layer of the convolutional neural network. As shown in Figure 19, the features of the input layer cannot separate the six types of working states. It can be seen that the input features cannot realize the classification of samples; the features of convolutional layer 2 can initially realize the division between each state, but state 3 (single slipper off fault) is doped part of the samples of state 4 (single slipper wear fault). The classification effect is not obvious. The features of convolutional layer 4 can basically realize the obvious division between each state, but state 4 (single slipper wear fault) is doped part of the samples of state 3 (single slipper off fault), which does not achieve effective fault diagnosis. The characteristics of the

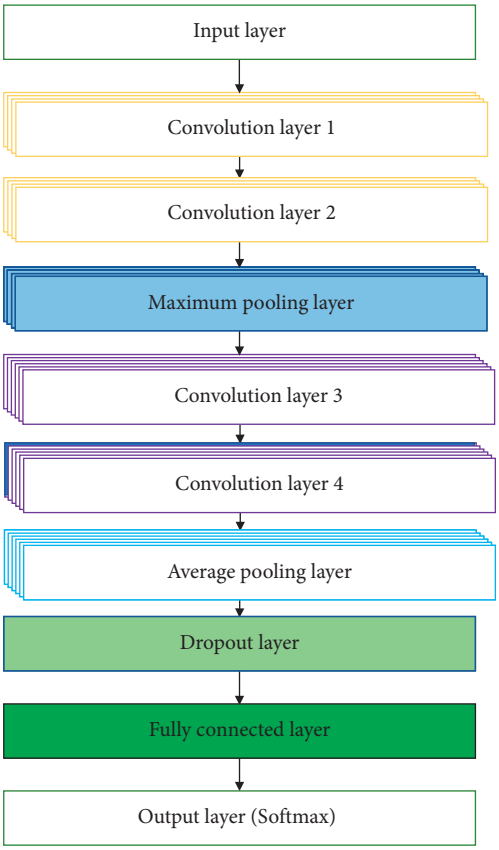

Figure 15: One-dimensional convolutional neural network structure.

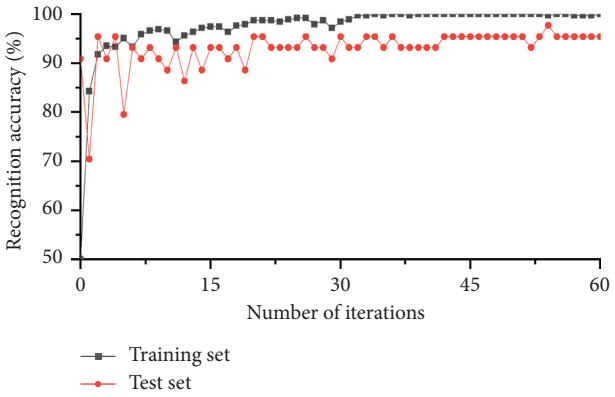

Figure 16: Change curves of sample recognition accuracy rate during model iteration.

output layer can completely realize the division between states and the effect is obvious. This shows that the EWT-CNN has powerful feature extraction and fault diagnosis ability.

5.6. Cloud Platform Realization of Fault Diagnosis Method for Axial Piston Pump. Traditional fault diagnosis algorithms mainly focus on local data acquisition of single or multiple devices and real-time fault diagnosis locally. This makes the equipment's condition monitoring and fault diagnosis system costly and cannot realize the remote monitoring and remote data analysis of the equipment. With the development of intelligent science and information science, people can realize modernized management of equipment and equipment monitoring automation, informatization, and interaction through intelligent means. This can ensure the normal operation of the equipment and improve the overall management and service level of the equipment, so as to ensure the

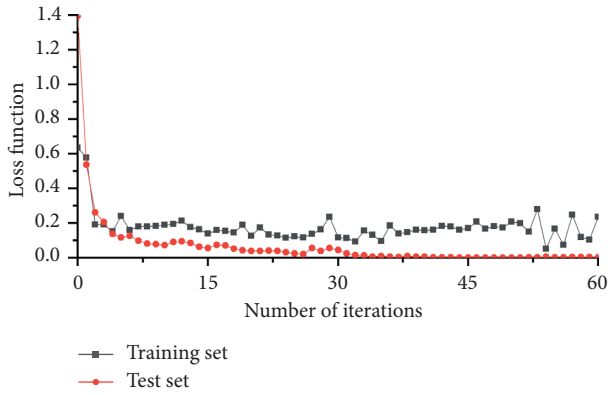

Figure 17: Sample loss function value change curves during model iteration.

Table 6: Comparison of recognition accuracy rate of different fault diagnosis methods.

Fault diagnosis method	Recognition accuracy (%)
EWT-CNN	99.51
EEMD-CNN	96.35
CEEMD-CNN	98.15

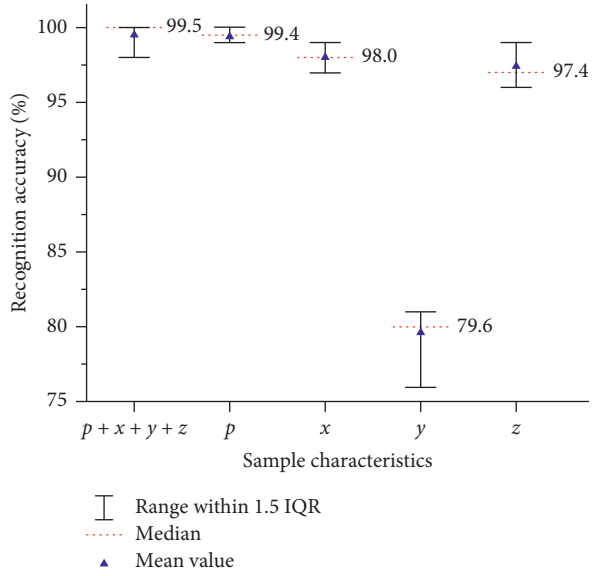

Figure 18: The accuracy rate of model recognition is affected by different characteristic parameters.

smooth operation of the equipment and improve the management level and service level of the equipment as a whole.

Therefore, this paper proposes an axial piston pump fault diagnosis algorithm based on cloud platform and deep learning. The deep learning algorithm is a new algorithm model based on big data. At the same time, the cloud platform is a new platform developed under the Internet technology. The platform can process a large amount of data in a short period of time and return the processing results to customers in an integrated form. In the past, multiple devices in a workshop needed a fault diagnosis system deployment mode of data processing and computing platform. Cloud platform can realize simultaneous online monitoring of multiple locations and multiple devices, with lower cost, faster processing speed, and higher platform utilization, which is suitable for deploying the fault diagnosis model of the axial piston pump in the cloud.

The fault diagnosis algorithm based on cloud platform proposed in this paper is mainly composed of three parts, as shown in Figure 20. The deployment mode of each functional module of the specific model is shown in Figure 21.

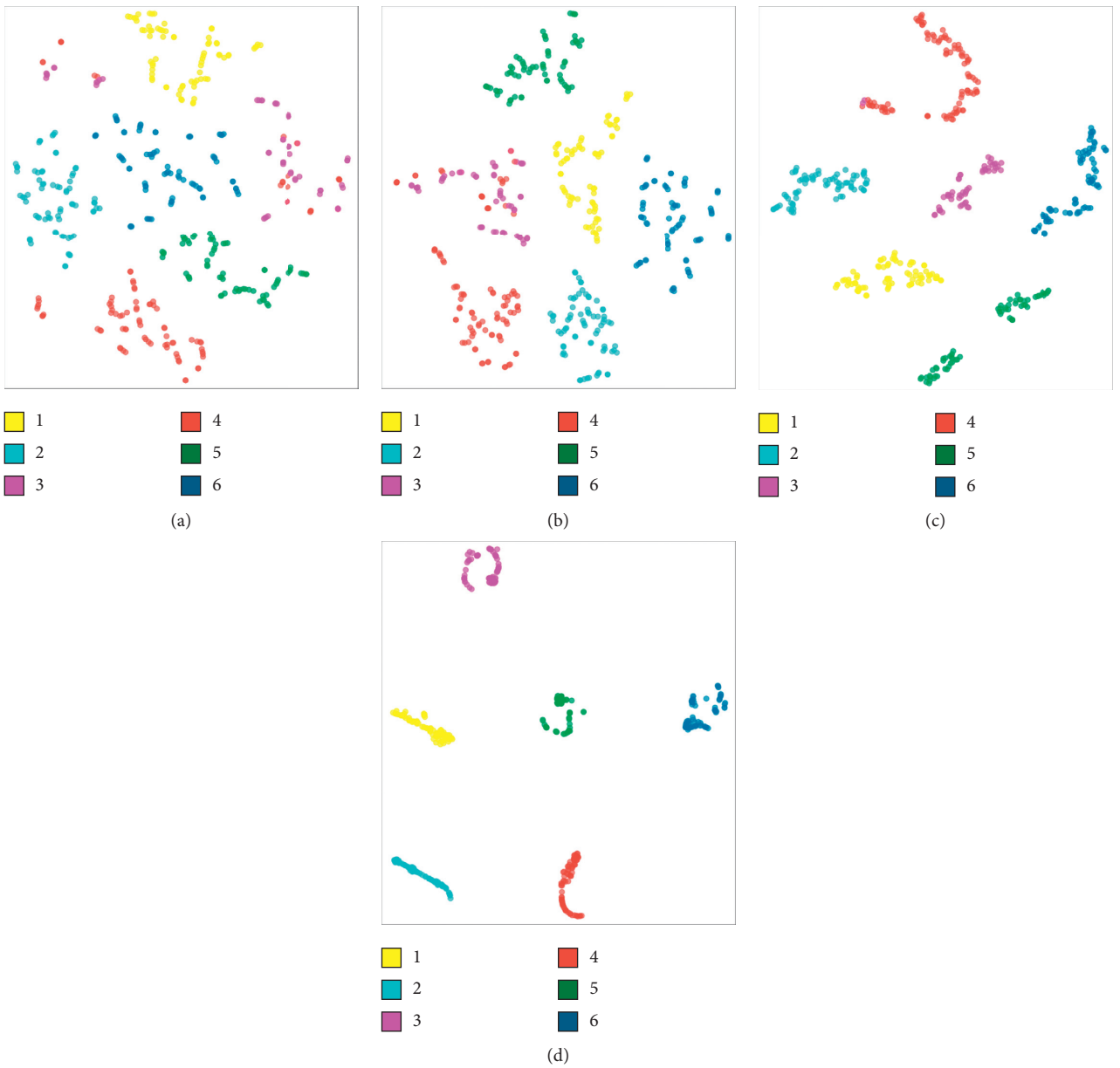

Figure 19: Visual output of different levels. (a) Input layer features. (b) Convolutional layer 2 features. (c) Convolutional layer 4 features. (d) Output layer features.

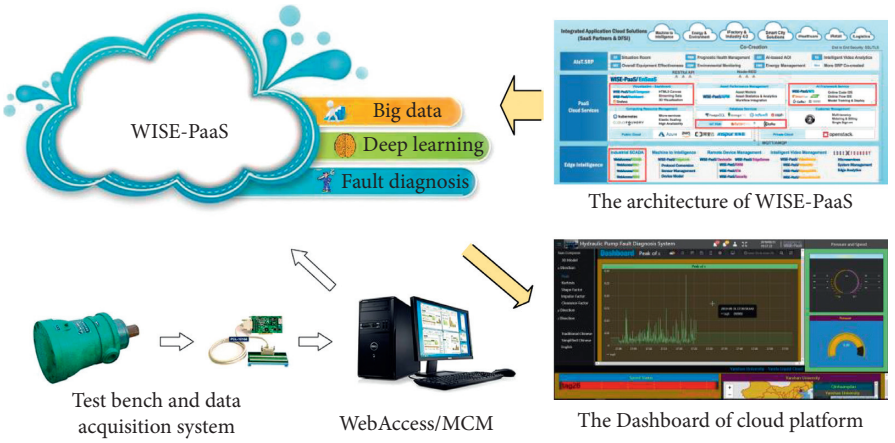

Figure 20: Hydraulic pump fault diagnosis system based on cloud platform.

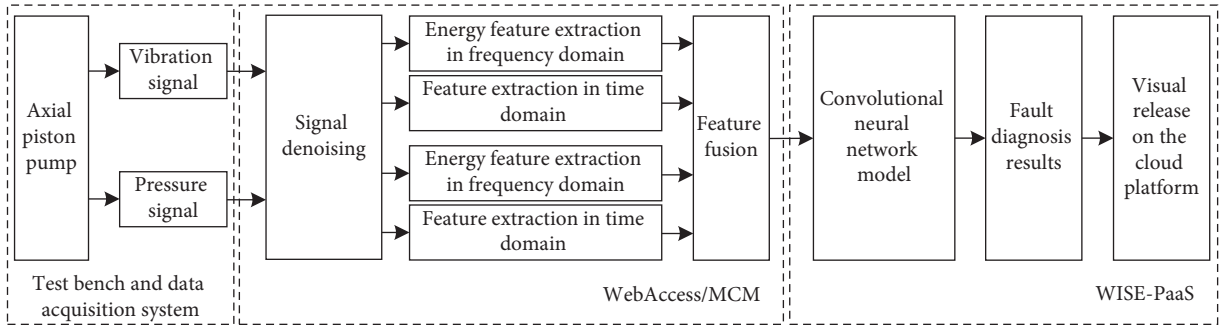

Figure 21: Cloud platform realization of the fault diagnosis method of axial piston pump.

(1) The axial piston pump data acquisition system is mainly used to collect the pressure signal and three directions vibration signals of the axial piston pump.

(2) Edge-side feature extraction and feature fusion algorithm based on WebAccess/MCM. Firstly, WebAccess/MCM denoises the original signal. Then the time-domain feature extraction and frequency-domain feature extraction are performed on the denoised signal. The next step is to perform feature fusion on the extracted features. Finally, upload the fused features to the WISE-PaaS cloud platform.

(3) 1D-CNN fault diagnosis model: deploy the trained fault diagnosis model to the WISE-PaaS cloud platform to realize online condition monitoring and fault diagnosis of the axial piston pump. The diagnosis results are displayed on the cloud platform in real time.

6. Conclusion

This paper proposes a fault diagnosis algorithm for axial piston pump based on EWT and 1D-CNN. Based on EWT, the original vibration signal and pressure signal of the axial piston pump are decomposed and denoised; then, extract and fuse the time-domain and frequency-domain features of the signal after denoising; finally, 1D-CNN is used to realize the fault diagnosis of axial piston pump on the cloud platform in real time. Through comparing the method proposed in this paper with the EEMD and CEEMD methods, the results show the following:

(1) Compared with the EEMD and CEEMD methods, the EWT-based signal decomposition and noise reduction method proposed in this paper can effectively eliminate the noise components of the axial piston pump vibration signal and pressure signal. It has better signal denoising effect.

(2) Using the method of time-domain and frequency-domain feature fusion, compared with the fault diagnosis method based on a single signal feature, it can obtain more comprehensive feature information of the axial piston pump. At the same time, the fault diagnosis method of axial piston pump based on multiple signals has higher recognition accuracy rate.

(3) As a deep-learning-based method, one-dimensional convolutional neural network can effectively extract the more abstract features of the vibration signal and pressure signal characteristic parameters of the axial piston pump, which can effectively improve the accuracy rate of the fault diagnosis and recognition of the axial piston pump.

(4) A fault diagnosis algorithm for axial plunger pump based on the industrial Internet of Things cloud platform is proposed. Deploying the fault diagnosis model on the cloud platform can not only improve the data processing capability of the algorithm but also reduce the hardware cost of the diagnostic system, so as to realize the unified management and fault diagnosis of multiple devices in remote places.

Data Availability

The data used to support the findings of this study are available from the corresponding author upon request.

Conflicts of Interest

The authors declare that there are no conflicts of interest regarding the publication of this paper.

Acknowledgments

This work was supported by the National Natural Science Foundation of China (Grant nos. 51875498 and 51475405) and Key Project of Natural Science Foundation of Hebei Province, China (Grant nos. E2018203339 and F2020203058). The support is gratefully acknowledged.

References

[1] Z. D. Du, J. M. Zhao, H. P. Li, and X. Zhang, "Research on fault diagnosis method of plunger pump based on SA-EMD-PNN," *Journal of Vibration and Shock*, vol. 38, no. 8, pp. 150–157, 2019.

[2] W. P. Ma, J. S. Ma, L. J. Cao, and S. J. Deng, "Simulation study of hydraulic system failure during adjustment of a rocket launcher," *Machine Tool & Hydraulics*, vol. 46, no. 17, pp. 180–184, 2018.

[3] L. Zhou, C. Han, L. Bai, and W. Li, "CFD-DEM bidirectional coupling simulation and experimental investigation of

particle ejections and energy conversion in a spouted bed," *Energy*, vol. 211, Article ID 118672, 2020.

[4] Y. Yang, L. Zhou, and W. Shi, "Interstage difference of pressure pulsation in a three-stage electrical submersible pump," *Journal of Petroleum Science and Engineering*, vol. 196, Article ID 107653, 2020.

[5] G. Peng, X. Huang, and L. Zhou, "Solid-liquid two-phase flow and wear analysis in a large-scale centrifugal slurry pump," *Engineering Failure Analysis*, vol. 114, Article ID 104602, 2020.

[6] S. M. Li, H. D. Guo, and D. R. Li, "Overview of vibration signal processing methods," *Chinese Journal of Scientific Instrument*, vol. 34, no. 8, pp. 1907–1915, 2013.

[7] S. Ye, J. Zhang, B. Xu, S. Zhu, J. Xiang, and H. Tang, "Theoretical investigation of the contributions of the excitation forces to the vibration of an axial piston pump," *Mechanical Systems and Signal Processing*, vol. 129, pp. 201–217, 2019.

[8] S. G. Ye, J. H. Zhang, and B. Xu, "A theoretical dynamic model to study the vibration response characteristics of an axial piston pump," *Mechanical Systems and Signal Processing*, vol. 150, Article ID 107237, 2021.

[9] S. M. Li and X. L. Li, *Modern Analysis Technology and Application of Vibration Signal*, National Defense Industry Press, Beijing, China, 2008.

[10] J. G. Zhang, Y. F. Li, and J. Q. Zhao, "Analysis of the transmission characteristics of ultrashort optical pulses based on short-time Fourier transform," *Laser Technology*, vol. 37, no. 1, pp. 52–55, 2013.

[11] L. S. Shi, Y. Z. Zhang, and W. P. Mi, "Application of WVD-based spectral kurtosis method in bearing fault diagnosis," *Journal of Vibration, Testing & Diagnosis*, vol. 31, no. 1, pp. 27–31, 2011.

[12] B. Y. Xu, Y. L. Liu, and X. D. Wang, "Random interference model and ARMA spectrum analysis of strip mill," *Journal of Vibration and Shock*, vol. 31, no. 7, pp. 1–3, 2012.

[13] S. Y. Yan, C. Liu, H. B. Zhao, and H. Wang, "Feature extraction of consciousness EEG based on wavelet packet decomposition," *Chinese Journal of Scientific Instrument*, vol. 33, no. 8, pp. 1748–1752, 2012.

[14] Z. Wu and N. E. Huang, "Ensemble empirical mode decomposition: a noise-assisted data analysis method," *Advances in Adaptive Data Analysis*, vol. 1, no. 1, pp. 1–41, 2009.

[15] J. Gilles, "Empirical wavelet transform," *IEEE Transactions on Signal Processing*, vol. 61, no. 16, pp. 3999–4010, 2013.

[16] J. Pan, J. Chen, Y. Zi, Y. Li, and Z. He, "Mono-component feature extraction for mechanical fault diagnosis using modified empirical wavelet transform via data-driven adaptive Fourier spectrum segment," *Mechanical Systems and Signal Processing*, vol. 73, pp. 160–183, 2016.

[17] M. Y. Zhao and G. Xu, "Feature extraction of transformer vibration signal based on empirical wavelet transform," *Automation of Electric Power Systems*, vol. 41, no. 11, pp. 63–69, 2017.

[18] K. Chai, M. J. Zhang, J. Huang, and Z. Y. Wang, "Hydraulic system fault diagnosis based on time-frequency characteristics and PCA-KELM," *Journal of PLA University of Science and Technology: Natural Science Edition*, vol. 16, no. 4, pp. 394–400, 2015.

[19] H. B. Tang, Z. C. Wang, and Y. Wu, "A multi-fault diagnosis method for piston pump in construction machinery based on information fusion and PSO-SVM," *Journal of Vibroengineering*, vol. 21, no. 7, pp. 1904–1916, 2019.

[20] S. Wang and J. Xiang, "A minimum entropy deconvolution-enhanced convolutional neural networks for fault diagnosis of axial piston pumps," *Soft Computing*, vol. 24, no. 4, pp. 2983–2997, 2020.

[21] S. Wang, J. Xiang, Y. Zhong, and H. Tang, "A data indicator-based deep belief networks to detect multiple faults in axial piston pumps," *Mechanical Systems and Signal Processing*, vol. 112, pp. 154–170, 2018.

[22] S. Y. Liu, Y. He, X. M. Li, M. L. Lu, and Z. D. Lu, "Evaluation method of hydraulic pump multi-information intensity characteristic state based on failure mechanism," *China Mechanical Engineering*, vol. 30, no. 12, pp. 1460–1473, 2019.

[23] W. L. Jiang, Z. B. Li, J. J. Li, Y. Zhu, and P. Y. Zhang, "Study on A fault identification method of the hydraulic pump based on a combination of voiceprint characteristics and extreme learning machine," *Processes*, vol. 7, no. 12, p. 894, 2019.

[24] Y. Lecun, Y. Bengio, and G. Hinton, "Deep learning," *Nature*, vol. 521, no. 7553, pp. 436–444, 2015.

[25] R. X. Chen, X. Yang, and L. X. Yang, "Rolling bearing damage diagnosis based on stacked sparse and noisy self-encoding deep neural network," *Journal of Vibration and Shock*, vol. 36, no. 21, pp. 125–137, 2017.

[26] Y. Lei, F. Jia, and X. Zhou, "A deep learning-based method for machinery health monitoring with big data," *Journal of Mechanical Engineering*, vol. 51, no. 21, pp. 49–56, 2015.

[27] W. Sun, S. Shao, R. Zhao, R. Yan, X. Zhang, and X. Chen, "A sparse auto-encoder-based deep neural network approach for induction motor faults classification," *Measurement*, vol. 89, pp. 171–178, 2016.

[28] S. Tang, S. Yuan, and Y. Zhu, "Deep learning-based intelligent fault diagnosis methods toward rotating machinery," *IEEE Access*, vol. 8, no. 1, pp. 9335–9346, 2020.

[29] S. Tang, S. Yuan, and Y. Zhu, "Convolutional neural network in intelligent fault diagnosis toward rotatory machinery," *IEEE Access*, vol. 8, no. 1, pp. 86510–86519, 2020.

[30] S. Wang, J. Xiang, Y. Zhong, and Y. Zhou, "Convolutional neural network-based hidden Markov models for rolling element bearing fault identification," *Knowledge-Based Systems*, vol. 144, pp. 65–76, 2018.

[31] C. Li, J. L. Li, D. H. Sun, Z. W. Lei, and Y. L. Yu, "Research on remote monitoring and fault diagnosis system based on Alibaba Cloud," *Modular Machine Tool and Automated Processing Technology*, vol. 1, pp. 76–78, 2020.

[32] Y. Song, D. Q. Wang, C. C. Fu, and Z. Y. Liu, "Research and development based on the remote monitoring system of workshop equipment," *Modular Machine Tool and Automatic Processing Technology*, vol. 7, pp. 86–88, 2018.

[33] S. Sivaranjani and R. Rajeswari, "Internet of things based industrial automation using brushless dc motor application with resilient directed neural network control fed virtual z-source multilevel inverter topology," *Wireless Personal Communications*, vol. 102, no. 4, pp. 3239–3254, 2018.

[34] Y. L. Ou, S. L. He, and C. F. Hu, "Research on rolling bearing fault diagnosis using improved majorization-minimization-based total variation and empirical wavelet transform," *Shock and Vibration*, vol. 2020, Article ID 3218564, 2020.

[35] J. Sun, *Research on Vibration Fault Feature Extraction and Life Prediction of Rolling Bearings*, Dalian University of Technology, Dalian, China, 2015.

[36] S. Tang, S. Yuan, and Y. Zhu, "Data preprocessing techniques in convolutional neural network based on fault diagnosis towards rotating machinery," *IEEE Access*, vol. 8, pp. 149487–149496, 2020.

[37] Z. X. Zhang, "The use of CNN deep learning model for facial expression feature extraction methods," *Modern Computer (Professional Edition)*, vol. 3, pp. 41–44, 2016.
[38] X. X. Zhu, *Research on Vehicle Speech Recognition Technology Based on One-Dimensional Convolutional Neural Network*, Anhui University, Hefei, China, 2017.
[39] W. J. Sun, *Research on Induction Motor Fault Diagnosis Method Based on Deep Learning Model*, Southeast University, Nanjing, China, 2017.
[40] J. L. Qu, L. Yu, and T. Yuan, "Adaptive fault diagnosis algorithm for rolling bearing based on one-dimensional convolutional neural network," *Chinese Journal of Scientific Instrument*, vol. 39, no. 7, pp. 134–143, 2018.